Wavefront Correction using Array of Fibre Optic Delay Lines
Fibre Array Construction and Analysis

by

Robert Bedington

Supervisor: Dr RM Myers

Submitted in conformity with the requirements
for the degree of MSci (Level 4 project)
Department of Physics
University of Durham

Abstract

Wavefront Correction using Array of Fibre Optic Delay Lines

Fibre Array Construction and Analysis

Robert Bedington

A method was developed for creating passively aligned, close packed linear arrays of single-mode fibres, for the purposes of developing an array of optical fibre delay lines for a prototype wavefront corrector. Characterisation techniques developed showed the fibres in the array to have an average core to core spacing of 150.6±3.7μm, 25.6μm larger than intended, and a range of deviations from linearity of 9.7±3.6μm. The range of tip angles of the fibres in the array was found to be 1.96±0.09 degrees, the range of tilt angles was 3.83±0.01 degrees, which if the array were to be aligned to a lenslet array of focal length 5mm, would cause a deviation of 368±1μm in the x direction and 188±9μm in the y direction. The spatial coherence of the fibres in the array was confirmed by interferometry.

A computer program was made to simulate output arrays of single-mode fibres, using Fresnel diffraction theory, and was used to model the array that had been constructed, and the interference patterns produced from the overlapping output light cones of the fibres in it. A Monte Carlo type simulation was used to vary the fibre parameters according to the uncertainties on the original measurements and the uncertainty on the angle of the fringes was found to be 1.0±0.1 degrees.

The array constructed is not sufficiently accurate for the proposed wavefront corrector but the construction, characterisation and modelling techniques developed all represent progress in the project.

Contents

Chapter 1

Introduction

First the concept of adaptive optics is briefly introduced, then the motivations of this project are explained and the objectives of this specific investigation are outlined.

1.1 Adaptive Optics

Adaptive optics (AO) are used within optical systems to correct incoming wavefronts that contain rapidly changing aberrations (distortions). This technology is used regularly on ground-based astronomical telescopes. Light from astronomical sources has to pass through the Earth's atmosphere before it reaches the telescope and since the atmosphere is made of many layers of rapidly moving air, all with different temperatures and thus different refractive indexes, so the image of the astronomical object becomes quite distorted [1].

Historically, this has not seemed particularly important. This was because distortions introduced by the telescope itself were more significant (e.g. expansion and contraction due to temperature changes, vibration induced by drive motors, wind, etc.) and as we shall see later, atmospheric distortion is most significant when using larger diameter telescopes. Over the past thirty years however, advances in telescope design and the development of active optics[1] have made the distortions induced mechanically in the telescope much less than those induced by the atmosphere, and have allowed telescopes with large primary mirror diameters (6 - 11m) to be built. Such telescopes benefit enormously from adaptive optics enabling them to produce diffraction limited images. [1]

ELTs (Extremely Large Telescopes), the next generation of optical telescopes, will have diameters of 30-100m and for these adaptive optics will be essential as the atmospheric distortion effects will be huge. Adaptive optics have also found military applications, allowing for better observations of satellites from ground based telescopes, accurate long distance laser weapons, and *'SuperVision'* eye wear for better than 20/20 vision [2]. Free space optical communication systems have been enhanced using AO [3], and together with optical coherence tomography, AO is used to image the human retina [4].

1.2 Project Motivations

All adaptive optics systems contain a wavefront corrector component. It is the purpose of this device to turn the distorted wavefront that enters the telescope into something as close to a plane wave as it is able to, using information it is given by the feedback and control loop that connects it with a wavefront sensor (see figure

[1]Technology which actively corrects for low frequency environmental effects on the telescope by adjusting the shape of the primary mirror with computer controlled actuators.

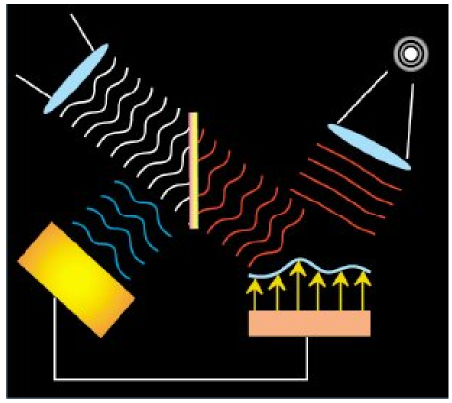

Figure 1.1: Simplified AO system, light enters from telescope top left, wavefront sensed by sensor bottom left, corrected by DM bottom right, diffraction limited image produced at top right [5].

1.1).

The most common form of wavefront corrector in an adaptive optics system, is a deformable mirror (DM). This is usually a segmented or flexible mirror membrane with actuators behind to change its shape to cancel out the aberrations introduced by the atmosphere. The more actuators the DM has, the better it is able to correct the wavefront.

With ELTs now under construction, a new generation of adaptive optics systems is required to enable these telescopes to be more than just light collecting buckets. One could produce a larger deformable mirror, with more actuators behind it, though this would be very expensive. Other possibilities include liquid crystal wavefront correctors or Micro-Opto-Electro-Mechanical (MOEM) technologies [6]. MOEMs would be small high resolution DMs or micro DMs built into the connected instruments (e.g. spectrographs), which would not correct the whole field of view of the telescope, only the small area being analysed [7]. This multiple DM approach is known as multi-object adaptive optics (MOAO).

In this project however, I look at a new approach to wavefront correction. Instead of a deformable mirror, the uncorrected image falls on an array of single-mode optical fibres. These fibres can be independently stretched to add path length and act as delay lines to produce a wavefront that is flat at the exit array of the fibres.

An optical fibre based system may also offer advantages in optical aperture synthesis interferometer setups where optical fibre delay lines connect up separate telescopes whilst correcting the path lengths, and where the required fields of view are small [8].

1.3 Investigation Objectives

It has already been demonstrated by Simon Morris, a previous MSci student in the research group, that single-mode fibres are capable of producing coherent phase delays at the frequencies required for AO [9]. His investigation however only dealt with an individual fibre. The technicalities and limitations of using arrays of single-mode fibres had not been investigated.

Arrays of multi-mode fibres are used in astronomical instrumentation (e.g. in spectrographs), but arrays of single-mode fibres do not seem to have been used much outside the field of communications and optoelectronics. Their use has been proposed however for a pupil filtering and remapping instrument which would be able to obtain high angular resolution and dynamic range images through atmospheric turbulence, whatever the wavelength [10]. This proposed instrument has an input lenslet array and fibre array that is very similar to that of the instrument proposed here.

The objectives of this investigation were to:

- Design and construct a demonstration array of single-mode fibres.
- To characterise and assess the accuracy of manufacture of the array.
- To produce a computer program to model the output of single-mode fibre arrays, and compare the model with the actual array.
- To work toward building such an array into a demonstration wavefront corrector.

Chapter 2

Background and Theory

The issues associated with atmospheric seeing are introduced followed by the current solutions to them. The new solution is then described, along with the theory required to model it.

2.1 Atmospheric Seeing Theory

Refractive index fluctuations in the atmosphere occur due to varying temperatures and cause eddies at various different scales from 1cm to 100m. This can be described mathematically using Kolmogorov Seeing Theory, from which it becomes apparent that there are three useful quantities for describing atmospheric seeing and that they are all inter-related. These three quantities are the coherence length, the coherence time and the coherence angle.

2.1.1 Coherence Length (Fried parameter), r_0

$$\theta = 1.22\frac{\lambda}{D} \tag{2.1}$$

$$\theta = 1.22\frac{\lambda}{r_0} \tag{2.2}$$

Astronomical image resolution depends on the diameter of the telescope producing it, and for a perfect instrument is given by equation (2.1) . Atmospheric turbulence puts a limit to the image resolution achievable by using just a passive telescope however. The coherence length, r_0, is defined as the diameter of a circular aperture over which the optical phase distortion has a mean square value of 1 rad^2 [11]. It essentially describes the diameter of telescope above which one would not see an increase in image resolution. In general then, without adaptive optics, it is not possible to obtain an astronomical image from a ground based telescope with a resolution greater than that given by equation (2.2). r_0 varies in different locations and atmospheric conditions, and indicates the resolution that the wavefront correcting elements will need to be able to work to, to produce diffraction limited images.

$$r_0 \propto \lambda^{\frac{6}{5}} \tag{2.3}$$

The coherence length varies with wavelength by the relationship in equation (2.3) [12]. This means that in the infra red regime the coherence length is longer than in the optical, making imaging easier.

2.1.2 Coherence Time, τ_0

$$\tau_0 = 0.314\frac{r_0}{\bar{v}} \tag{2.4}$$

The coherence time corresponds to the time over which changes in atmospheric

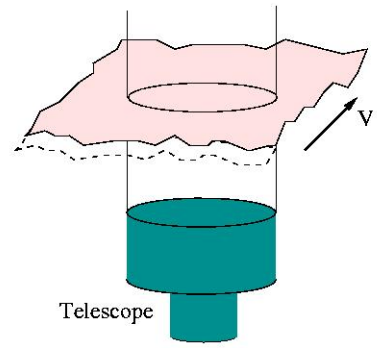

Figure 2.1: Turbulence can usually be modelled by fixed phase variations blowing across the field of view of the telescope [13].

turbulence become significant; the time it takes for a patch of atmosphere to blow across the path of the telescope (see figure 2.1). Coherence time is related to the average wind velocity, $\bar{v}$, by equation (2.4) [12].

$$\tau_0 \propto \lambda^{\frac{6}{5}} \tag{2.5}$$

The coherence time indicates the speed at which the adaptive optics system will need to operate to keep the wavefront plane (corrected), and since it is proportional to r_0, it varies with wavelength in the same way, see equation (2.5) [12].

2.1.3 Coherence Angle (Isoplanatic Patch size), θ_0

$$\theta_0 = 0.314\frac{r_0}{\bar{h}} \tag{2.6}$$

The coherence angle refers to the range of angles light can enter the telescope from, for which the turbulence can be considered to be the same (see figure 2.2) and is related to the height at which the turbulence occurs, $\bar{h}$, by equation (2.6).

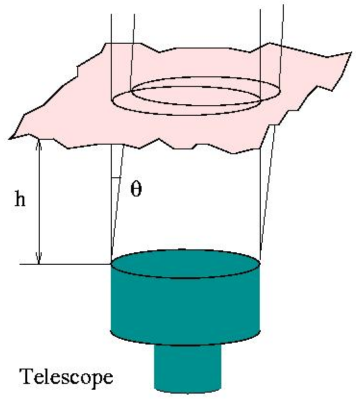

Figure 2.2: Isoplanatic angle; the turbulence light experiences varies with the angle it approaches the telescope at [13].

$$\theta_0 \propto \lambda^{\frac{6}{5}} \tag{2.7}$$

The coherence angle indicates how much of the field of view will be corrected and thus how close the object under observation needs to be to the guide star for the adaptive optics to be effective (explained later). Like the the coherence time it is proportional to r_0 and so varies with wavelength in the same way, see equation (2.7) [12].

2.1.4 Strehl Ratio

$$S \approx e^{-(\sigma_p)^2} \tag{2.8}$$

The Strehl ratio is the ratio of the actual peak intensity to the theoretical maximum intensity of the image. It is used to assess the quality of seeing and the performance of adaptive optics. It can be approximated by equation 2.8, where σ_p is the standard deviation of the phase, or fitting error of the wavefront corrector

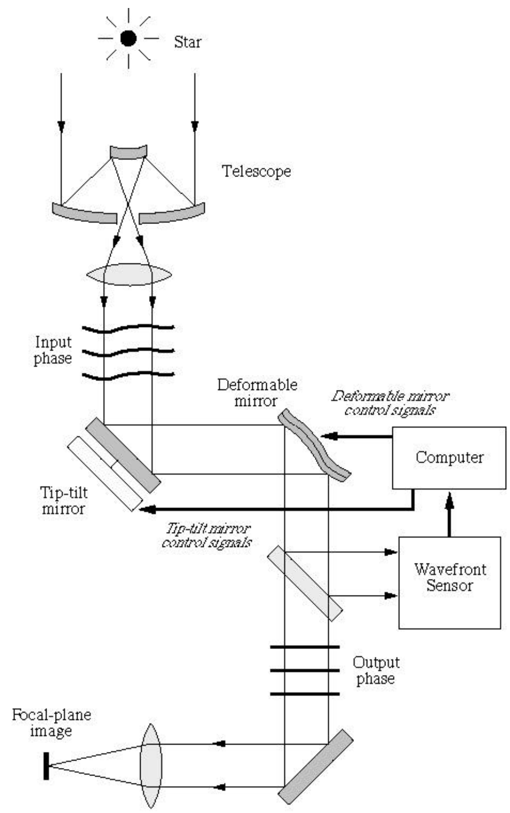

Figure 2.3: Schematic of typical AO setup [14].

(explained later) [11].

2.2 Conventional Adaptive Optics

Technology for correcting telescope images for the effects of atmospheric distortion.

2.2.1 Overview

The basic series of processes of an Adaptive optics system is shown in Figure 2.3. Light collected from a telescope is focused into a collimated beam onto a tip tilt

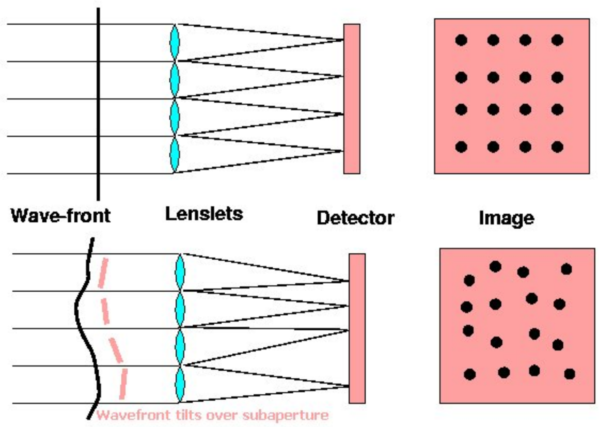

Figure 2.4: A Shack-Hartmann wavefront sensor breaks down the wavefront into many subapertures, each with a net tip or tilt. These are focused onto a CCD by lenslets, tiny lenses in an array. From the displacement of the foci these tips and tilts induce, the detector can approximate the distortion on the wavefront [13].

mirror. This mirror can tip and tilt to remove the large first order image aberrations, reducing image motion. It is able to do this from the information it is given by the control system. This first order corrected wavefront is reflected onto a deformable mirror, which removes the higher order aberrations by deforming to cancel the shape of the incoming wavefront, so the reflected light is plane. Again this device receives its instructions from the control system. The corrected plane wavefront from the deformable mirror is projected onto a beam-splitter, which divides the light between the output image plane and a wavefront sensor [11].

2.2.2 Wavefront Detection

The wavefront sensor is typically a Shack-Hartman device; a lenslet array which breaks up the beam into lots of small beams that are focused onto a CCD. When a distorted wavefront falls on the lenslet array, the local wavefront over a single lenslet will be approaching at an angle and so the beam will focus to a slightly different point on the CCD. The control unit can calculate from this data by how much the wavefront is distorted and how to adjust the deformable mirror accordingly (see figure 2.4) [15].

Alternative wavefront sensors include curvature sensors and interferometric based methods, such as the shearing interferometer and the pyramid wave front sensor [13].

A wavefront sensor can only accurately measure the aberrations if it has sufficient photons to sample, so the science object must either be bright, or within the coherence angle of a bright object (an NGS, Natural Guide Star). If neither of those conditions are satisfied (which is quite likely) a laser can be projected into the atmosphere where it backscatters light [16] or excites sodium atoms to emit light [17] to simulate a bright star and is called a Laser Guide Star (LGS).

2.2.3 Wavefront Correction

$$\sigma_{fit}^2 = \kappa \left(\frac{D}{n_{actuators} r_0} \right)^{\frac{5}{3}} \tag{2.9}$$

As mentioned previously, wavefront correction at the deformable mirror works by having a number of actuators behind the mirror controlling its shape. The number of these actuators/correction elements and the number of degrees of freedom each element has dictates the resolution to which the wavefront can be corrected. If there are more actuators, the wavefront corrector is able to correct smaller aberrations as well as the large ones, so the image is less distorted. The size of the

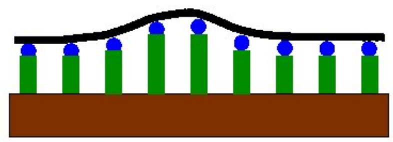

Figure 2.5: Side view of monolithic deformable mirror, actuators are in green [13].

atmospheric induced aberrations are related to the coherence length of the atmosphere so the fitting error for wavefront correction is given by equation (2.9) where D is the telescope diameter, r_0 is the Fried Parameter (coherence length), $n_{actuators}$ is the number of actuators and κ is the fitting error coefficient, which depends on the influence function of the corrector (discussed presently) [11].

A basic deformable mirror wavefront corrector is a grid of mirror sections with push-pull piezoelectric piston actuators behind each one. This of course creates discontinuities in the wavefront between the section boundaries and so a high fitting error coefficient $\kappa = 1.26$. If each piston is given tip-tilt capability as well (i.e. another two degrees of freedom) then there is a significant improvement, $\kappa = 0.14$, such is the DM used in the NAOMI system [18]. Alternatively if a thin mirror membrane is put over an array of piston actuators, a monolithic DM (figure 2.5) is created with $\kappa \simeq 0.28$ (depending on influence function)[11].

2.3 Optical Fibre Wavefront Corrector Proposal

For the optical fibre wavefront corrector proposed in this project, the distorted wavefront would arrive at a lenslet array that would break it up and focus it down into the fibre cores of an array of single-mode optical fibres. The fibres would then be stretched independently to introduce correcting path lengths for each subaperture producing an overall corrected wavefront. The number of fibres would be the num-

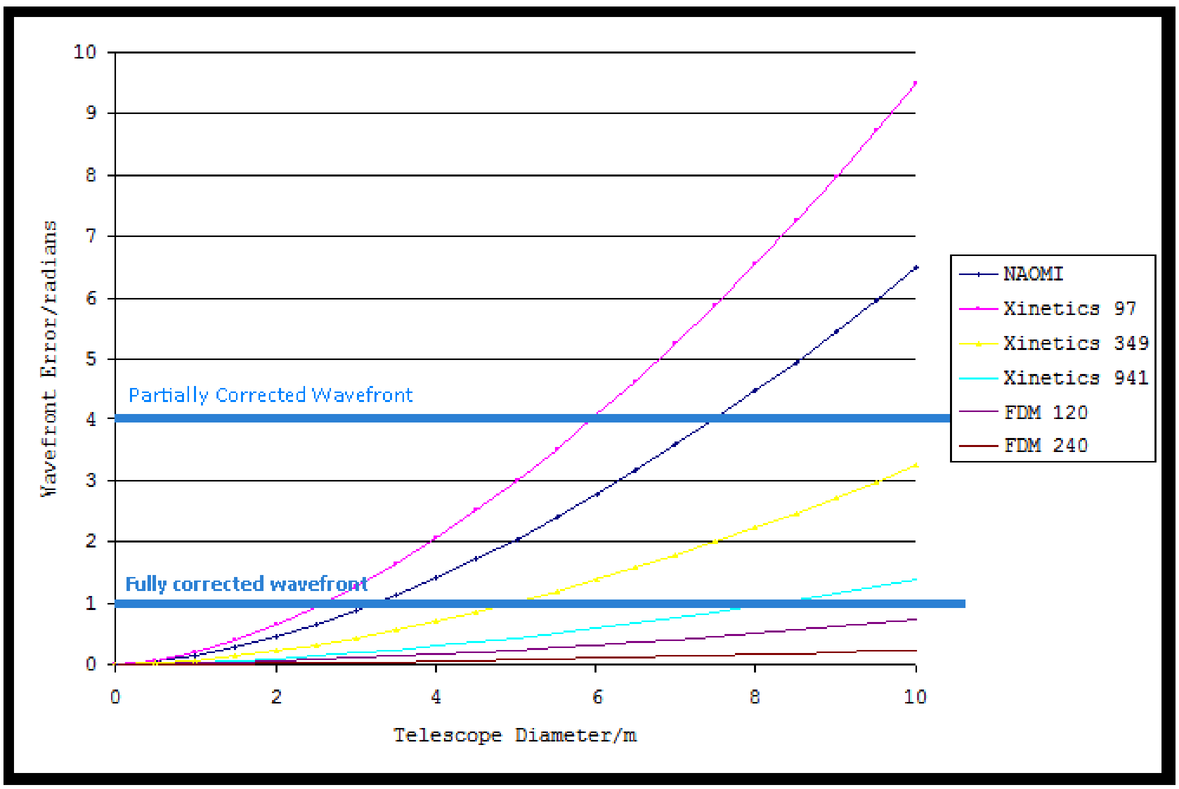

Figure 2.6: Wavefront fitting error versus telescope diameter for three types of deformable mirror. FDM 120 and FDM 240 show wavefront fitting errors for fibre wavefront correctors with 120x120 and 240x240 lenslet arrays respectively. Both lenslet arrays are commercially available. [6].

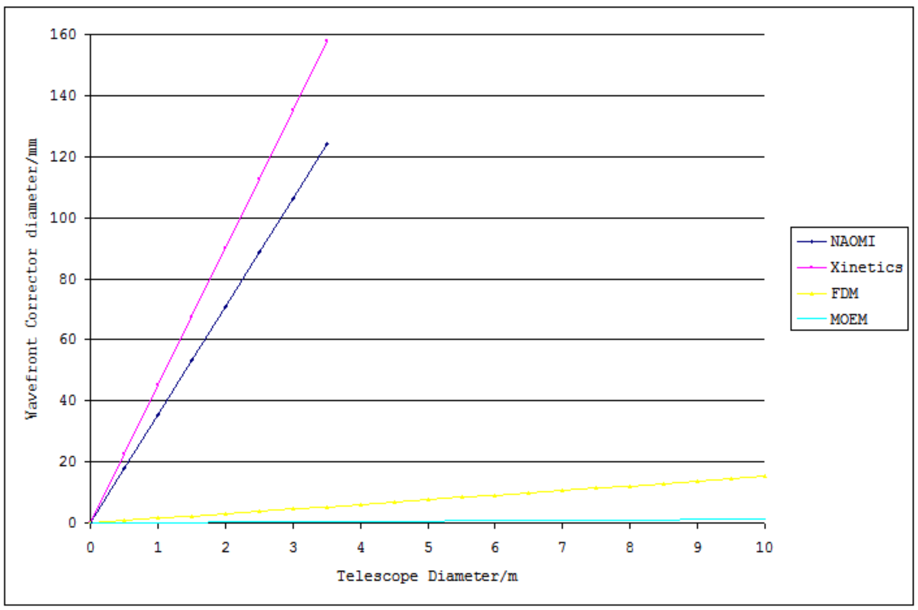

Figure 2.7: Physical dimensions of wavefront corrector required for 0.5 rad^2 wavefront fitting error for different telescope diameters. Fibre Deformable Mirror (FDM), the proposed optical fibre wavefront corrector, assumes a 100-micron pitch, MOEM assumes 17-micron pitch, Xinetics has 7mm pitch, NAOMI has 7.62mm pitch [6].

ber of actuators and the corresponding κ value would be $\kappa \approx 1.26$ since it would be similar to the push-pull only piston technology.

To make this technology viable and competitive with continuous sheet and tilt capable deformable mirrors, it would have to be able to have many sub-apertures, at least 5 per r_0 aperture [6]. Figure 2.6 compares the wavefront fitting error of a 120x120 and a 240x240 optical fibre wavefront corrector with various current DMs, as a function of telescope diameter. As can be seen, for larger telescopes the fibre based system has considerably lower fitting errors than the existing DMs. This is one reason why optical fibre array based wavefront correctors could be considered for ELTs. Another selling point is the small physical size of the proposed corrector compared to current technologies. Figure 2.7 shows how the size of an optical fibre based wavefront corrector would vary with telescope diameter compared to existing technologies and MOEMs, for the same level of correction.

2.3.1 Lenslet-fibre Coupling

The distorted wavefront would first fall on a lenslet array, a grid of tiny lenses exactly like those found on a Shack-Hartmann wavefront sensor (see figure 2.4), except instead of focusing onto a CCD, it would be exactly aligned to focus into the fibre cores of an array of single-mode fibres. This presents a few problems immediately however. As the Shack-Hartmann wavefront sensor demonstrates, the foci produced from a distorted wavefront are displaced by a certain amount depending on the wavefront tip and tilt over the subaperture. If over one subaperture of the optical fibre wavefront corrector, the wavefront were sufficiently distorted, the focus

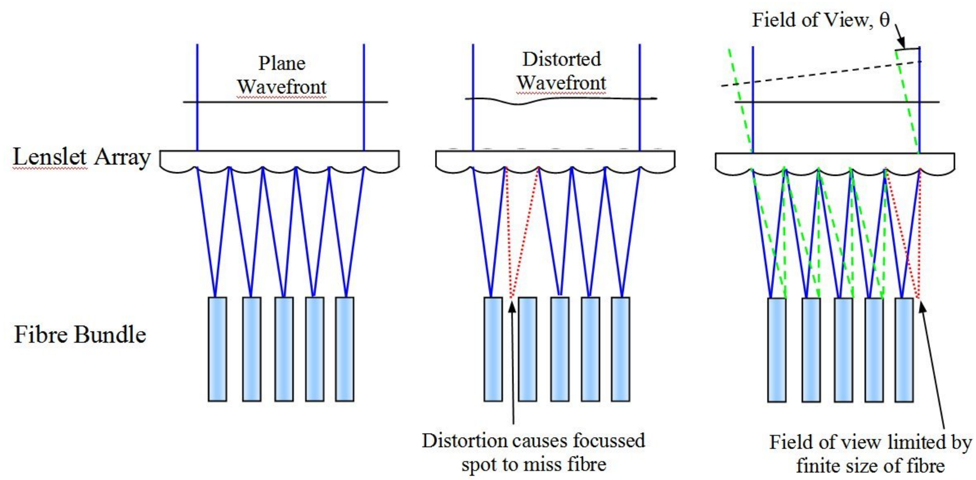

Figure 2.8: If the tip/tilt is too large over one subaperture, then light fails to couple into the fibre.[6].

could fall outside the core diameter of the fibre. If this happened the light would not be coupled (see figure 2.8). The lenslet focal length and diameter, and the numerical aperture of the fibre would need to be chosen to minimise this effect as much as possible.

$$d = 2.44\frac{\lambda f}{D} \tag{2.10}$$

The diffraction limit of even perfectly made optics means that the focus of each lenslet lens is an airy disk with a diameter, d, given by equation 2.10 [19]. If the lenslet has lenses with diameter, $D = 0.125$mm and focal length $f = 0.5$mm using visible light wavelengths (λ=400-780nm) [20] they would have Airy disk diameters of 4-8μm at their foci.

This compares to the fibres quoted mode field diameter ($\approx$ core diameter) of

4.3μm so there is little room for variation and unless the coupling is very accurate much light will be lost [21]. Even the most accurately aligned setup however will experience losses since there is a mismatch between the Airy pattern produced by the lens and the Gaussian field inside the fibre. This produces a theoretical upper limit of 78% of the incident light which can be coupled into the fibre and that doesn't include light lost into the cladding due to imperfections in the fibre [22].

If displaced foci from the fibre cores proves to be a significant issue in the lenslet-fibre coupling, one could have a Shack Hartmann wavefront sensor before the corrector to map where the foci will fall, and somehow adjust the position of the fibres accordingly, perhaps using electrostatic forces as described in the fibre array making process later in section 2.4.2. If the behaviour of the wavefront corrector was predictable enough, this wavefront sensor could also be used to calculate the required stretches to correct the wavefront, though it is more common to have the wavefront sensor after the corrector so that it corrects any additional distortions introduced by the wavefront corrector itself. If one were to have two wavefront sensors however, one before and one after, it would decrease the amount of light available for the final image.

The wavefronts we have considered so far, are just the on-axis ones from the guide star or laser guide star. This is rarely the object of scientific interest, which is usually a faint object within the coherence angle of the guide star. This science object is generally off-axis. In fact, its wavefront may be several arcminutes off-axis which is significantly bigger than typical atmospheric tilts which are about a single arcsecond. It also means that it will not focus down into the fibres correctly (see far right diagram in figure 2.8) meaning the field angle is likely to become scrambled for stars more than a few milliarcseconds off-axis. This is perhaps the biggest problem with the wavefront corrector proposal. If it is found that this field of view cannot be improved upon then the wavefront corrector's uses in astronomical adaptive optics will be limited.

One potential application however would be in MOAO as discussed in the introduction. Here there are many small adaptive optics devices looking at individual objects and not the entire field of view. Another application would be in the field of astronomical interferometry where many telescopes are used to synthesise parts of a much larger telescope. The proposed fibered large interferometer on top of Mauna Kea, connecting up the existing telescopes there is an example of this [23]. To create a large virtual telescope like this one can only use a very narrow field of view at the centre of the telescope to produce the necessary overall curvature. The narrow field of view of the proposed instrument might be compatible with the optical fibre wavefront corrector, indeed it might be preferable to a conventional DM here since optical fibres would be used anyway as delay lines (see next section) connecting the separate telescopes and correcting the path lengths between them [23].

2.3.2 Optical Fibre Delay Line

When an optical fibre is stretched along its axis, the core changes shape so it is longer and thinner and its refractive index changes also. This combined effect results in an increased path length for light travelling along it. Unfortunately the effect can be different on different polarisation states, but polarisation preserving fibres with asymmetric cladding that preserve the core shape have been developed, which minimise this effect [6].

Optical fibre delay lines are not a new concept. As mentioned earlier, they are used in astronomical interferometry to equalise optical path distances between telescopes as they track objects across the sky. For this purpose they may have to be stretched several tens of metres which can be achieved with a large expanding drum, around which the fibre is wound many times [24]. The rate at which the fibres would have to be stretched for adaptive optics however would be much faster than the gradual stretch required for interferometry. Investigations show that single-mode fibres can have the applied stretch varied at a rate of 500Hz and still demonstrate a coherent path difference, which should be fast enough for an adaptive optics system [9].

In the optical fibre wavefront corrector, each fibre would require a separate stretcher, but an advantage of using optical fibres is that these fibres and stretchers can be physically arranged in the cheapest most convenient manner, unlike deformable mirror actuators which have to be packed tightly together behind the mirror [6].

2.3.3 Optical Fibre output

Using optical fibres is also useful as the output can be located wherever is convenient. It can also be spliced/ redirected, etc. with existing fibre optics technologies. For wavefront sensing, conventional sensors could be used, or adjacent lenslets could have their light combined and the fibres adjusted until interference fringes are observed (though light levels may be too low for this to work effectively). Further-

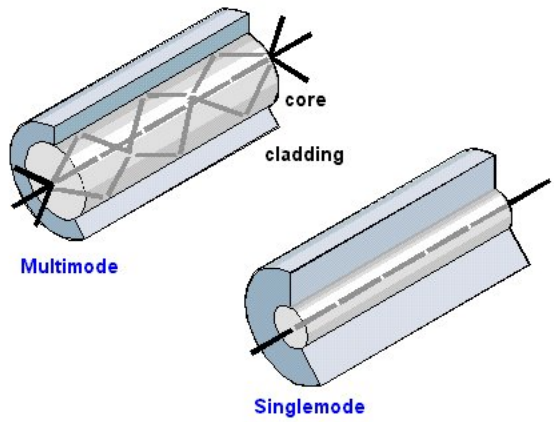

Figure 2.9: Modal dispersion - in multi-mode fibres light has different paths it can take, which have different lengths, unlike in single-mode fibres where there is only one possible path. [25].

more the fibres do not have to be kept in the same relative positions to each other, for example they could be arranged linearly for a quicker readout from a CCD [6].

Recreating an image from the light exiting the fibres may prove difficult however, as the light will be in phase and may produce complicated diffraction patterns [6]. This is something that will need to be investigated later in the project.

2.4 Optical Fibres

Step index optical fibres transmit light by total internal reflection between the core and the cladding, which surrounds the core and which has a slightly lower refractive index.

2.4.1 Single-Mode Fibres

Single-mode fibres differ from multi-mode fibres by allowing the light (above a certain wavelength) that enters only one possible mode of propagation, one path it can take to get to the other end, and this is due to their small cross sectional diameter. In multi-mode fibres there are several paths that the light can take and these have different lengths, meaning that the relative phase of two beams entering the fibre is not always preserved upon exiting as the beams could travel different distances along the fibre to reach the end (see figure 2.9). The difference in distance travelled for different modes is the modal dispersion. For a wavefront correction device single-mode fibres are essential as it needs to have complete control over the path length of the light that travels along it.

$$NA = \sqrt{n_1^2 - n_2^2} \tag{2.11}$$

A consequence of having just a single mode to travel along is that there is a smaller acceptance angle, θ, for light to enter the fibre at an off-axis angle and still be propagated through the it. The light gathering power of an optical fibre is generally quoted in terms of Numerical Aperture, NA, which for a step-index fibre is measured using equation 2.11, where n_1 is the refractive index of the core and n_2 the refractive index of the cladding [26].

$$NA = n_i \sin\theta \tag{2.12}$$

In most optical systems the numerical aperture would be related to the acceptance angle by equation 2.12, where n_i is the refractive index of the immersing medium (for air $n_i \approx$1) [19]. For single-mode fibres however this can only be considered as

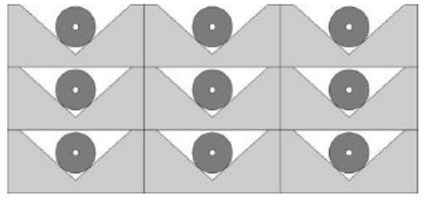

Figure 2.10: Alignment using etched v-grooves [31].

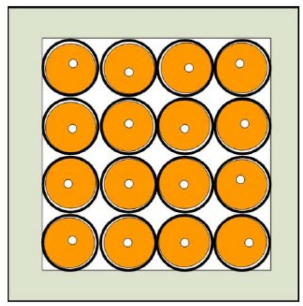

Figure 2.11: Alignment using micro-ferrules [31].

an approximation since the fibres are too thin compared to the wavelength of light travelling along them to be able to use geometric optics to model them and instead they have to be considered as electromagnetic structures.

2.4.2 Arrays of Fibres

Arrays of optical fibres are found in many instruments including spectrographs. These are usually made from multi-mode fibres which can be made into 1D arrays by inserting them in v-grooves etched in sheets of silicon. The sheets can then be stacked to produce 2D arrays (see figure 2.10) [27] [28]. Alternatively, fibres can be inserted into ferrules (e.g. hypodermic syringe needles) and then stacked to build an array (see figure 2.11) [29]. Hexagonal arrays are also used in these applications and provide better light collecting.

Arrays of single-mode fibres however are far less common. The fibres are significantly smaller and so must the tolerances in array construction be also, in order to couple light effectively. The main problem associated with the passive alignment construction techniques is that they rely on the fibres themselves being made to a high degree of accuracy, particularly the diameter of the fibre cladding and the eccentricity of the fibre core inside the fibre (i.e. how far the core is off the central axis of the fibre) [30]. The core eccentricity of the fibre used in this investigation is quoted as being $<1.0\mu$m [21]. Methods developed for manufacturing arrays of single-mode fibres are quite elaborate. One such method has the fibre tips coated with metal and inserted into micro-holders with four electrodes. The fibre is electrically grounded and voltages applied from the electrodes to create electrostatic forces to position the fibre. The holder is filled with UV curable glue so the fibre can be fixed into place, and once cured the whole assembly is polished to maximise the light that can be coupled into it [31].

2.5 Modelling single-mode Fibres

The optics theory required for producing a computer simulation of an array of single-mode fibres

2.5.1 Fresnel Diffraction Theory

$$U = \frac{E_0 e^{ikr}}{r} \tag{2.13}$$

The output ends of single-mode fibres can be approximated as point sources, since they only have one optical path they can transmit only an intensity and a phase and not an image. The Huygens-Fresnel principle describes the complex amplitude U from a spherical wave, with intensity E_0 and wave vector k, emitted by a point source a distance r away by equation 2.13 [32].

$$K = \frac{1}{2}(1 + \cos\theta) \tag{2.14}$$

Directionality can be applied to this term by multiplying it by an obliquity factor K, equation 2.14, so that the intensity is less, the greater the angle θ is from the on-axis position [19]. On top of this one must apply a Numerical Aperture.

2.5.2 Optical Interference

$$I = I_1 + I_2 + 2\sqrt{I_1 I_2}\cos\delta \tag{2.15}$$

Optical interference is observed and required at several points in this investigation. For two monochromatic beams to interfere and produce a stable pattern, they must have (very nearly) the same frequency. They need not be in phase but they have to be spatially and temporally coherent (have a constant phase difference). White light too can be shown to produce observable interference, since the component reds will interfere with reds and blues with blues, though the pattern produced will not be as sharp as for monochromatic light. For this investigation only monochromatic light will be used so the optical path lengths will not have to be equalised exactly, but for future, white light experiments where identical path lengths are required, techniques have been developed for equalising short (1-2.75m) lengths of single-mode fibre to 2.28$\pm$1.53μm [33].

The irradiance (average energy per unit area per unit time) of two interfering beams is given by equation 2.15, where I_1 and I_2 are the irradiances of the two component beams and δ is the phase difference between them. From this one can see that constructive interference occurs when the phase difference is $2n\pi$, and destructive interference for $(2n+1)\pi$ where n is any integer. One can also see that the contrast is going to be greatest when $I_1 = I_2$ since the minimums will be exactly zero. To get clear fringes then, the two beams to be interfered need to be about the same size and power.

The interference fringes formed from a collection of point sources can be found by summing together the complex amplitudes due to each source at each point on the image plane (see section 2.5.1). The square modulus of the complex amplitude at a point is the intensity of the light at that point.

Chapter 3

Experimental

First the fibre array design and manufacture is discussed, then the characterisation methods and other components. Finally the computer program to model the array is introduced.

3.1 Fibre Array Design

Since pre-made single-mode fibre arrays are not readily available, the array had to be constructed in the laboratory. For a proof of concept demonstration, a passively aligned linear array of 6-10 fibres was considered appropriate.

3.1.1 Passive Alignment

The fibres have a cladding diameter of $125\pm1\mu$m [21]. With the lack of any ferrules designed for single-mode fibres, a simple way to ensure regular spacing between fibres was to close pack the jacket-less fibres flush against each other, provided a compatible lenslet array could be acquired.

All passive alignment methods rely on the cores of the fibres being well centred within the cladding, see figure 2.11. If the core positions are off-axis, then even an array of perfectly close packed fibres would produce an irregularly spaced array [30].

3.1.2 Lenslet Array Compatibility

The spacing of the fibres in the array needs to match the spacing of the lenslets in the lenslet array. For the purposes of this project a sampler slide of lenslet arrays was available containing a range of linear and 2D lenslet arrays on it. The pitch (inter-lenslet spacings) of the arrays were determined by attaching the sampler slide onto a micrometer scaled translational stage under a microscope. The equipment was arranged so that the translation axes lined up with the sides of the observation monitor of the microscope. The position of the micrometer when a lenslet was lined up with the edge of the monitor was recorded. The stage was moved until 100 lenslets (or fewer if the array had less than 100) had passed and a similar measurement was performed. The average pitch was determined from the difference between the two measurements divided by the number of lenslets passed. As well as the required 125μm spacing, the sampler was found to have arrays of pitch 40, 140 and 250μm (measured to an accuracy of at least 0.1μm) in various forms, linear, square 2D, hexagonal 2D etc.

To find the focal length of the lenslets, the lenslet array was placed under a microscope with a collimated light beam passing up through the lenslets and into the microscope lens. The difference in position for focusing the microscope on the

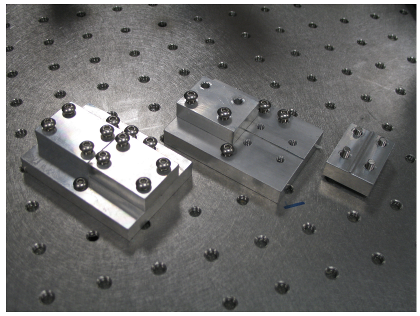

Figure 3.1: Aluminium fibre-holding block.

lenslets themselves and on the focus of light that they were producing from the collimated beam was the focal length of the lenslet. Error on the measurement due to backlash in the adjustment system was minimised by recording the position of the microscope lens when adjusting in one direction only.

The 125μm pitch square 2D array was found to have a focal length of 5.54$\pm$0.08mm. The lenslet array was not used again in this investigation.

3.2 Fibre Array Construction

To achieve the design specification of a linear array of 6 to 10 buffer stripped, close packed, single-mode fibres, several construction techniques were attempted.

3.2.1 Cleave and Hold

Initially the fibres were cut roughly to length using scissors and the protective outer jacket was removed using either dichloromethane or a mechanical fibre stripping tool. The ends of the fibres were cleaved flat by first scoring them with a diamond tipped pen where the break was to be made, then pulling along the axis of the fibre.

The fibre tips were then checked using a 10X magnification microscope to see if the cleave was uniform over the core of the fibre (to maximise light coupling) and if not, cleaved again until it was. Initially aligning the fibre ends together was attempted with an aluminium block with a groove ten fibres wide, see figure 3.1. Ten fibres were laid side by side in the groove and a tightly fitting lid was screwed on to secure the fibres in place. Unfortunately the fibres did not lie flat easily, and if they were they would become misaligned in the other dimension (end to end). It was also not possible to adjust the position of one fibre (to try and correct for this) without also moving the others. Furthermore the tolerances to which the holder was made were not sufficiently high to be able to force the fibres into position by clamping. Not that this mattered since clamping caused the fibres to break, even when padding strips of various materials were inserted also.

3.2.2 Glue and Polish

It was discovered however that applying blu-tak, or a small amount of moisture to the fibres until they were slightly tacky would cause them to be held together loosely in a row in what was essentially a linear array. Aligning five or more fibres sufficiently well, applying glass bond and then curing the bond with UV light however proved too difficult. The final method arrived at was to strip 5cm of protective coating (buffer) from one of the ends of each fibre. The stripped ends were then aligned so that they were flat and parallel, using vernier callipers to hold them in place but not necessarily with their ends flush. Norland optical adhesive was then applied to them and a UV lamp was used to cure the glue and hold the fibres in this configuration. The fibres were only roughly cut, rather than carefully cleaved.

A uniform finish for good light coupling was obtained after the curing process by polishing the end of the array, and thus the fibre ends, with fibre polishing paper.

To prevent the fibres breaking during polishing, they needed to be mounted in a holder. Initially brass sheets and glass microscope slides were tried, but the brass did not maintain the linear alignment well, and the glass seemed to leave deposits on the polishing paper which scratched the fibre ends. Silicon v-grooves, as used for multi-mode fibre arrays were also tried, but the single-mode fibres, being smaller than multi-mode fibres, did not align accurately in the grooves as they had room to move around. The most satisfactory solution was to insert the fibre array into a 31.5cm long 2mm diameter stainless steel ferrule and hold it in place with optical glue, with the fibre array just protruding slightly out the end. The ferrule could then be inserted in a polishing puck and polished on wet sheets of fibre polishing paper of increasingly finer grade until there were no surface imperfections visible when viewed under 10X magnification. The long tube provided stain relief for the fibres, as earlier attempts suffered many breakages of fibres at the point where the buffer had been stripped away. The array consisted of ten fibres, eight approximately one metre lengths and two approximately two metre lengths to allow enough fibre for stretching tests to be performed on them.

3.3 Characterising the Array

Once the array had been made, extensive testing was performed to determine the quality of the array produced. Quality was assessed by measuring the relative positions of the ends the fibres, the angles at which the fibres were pointing and the

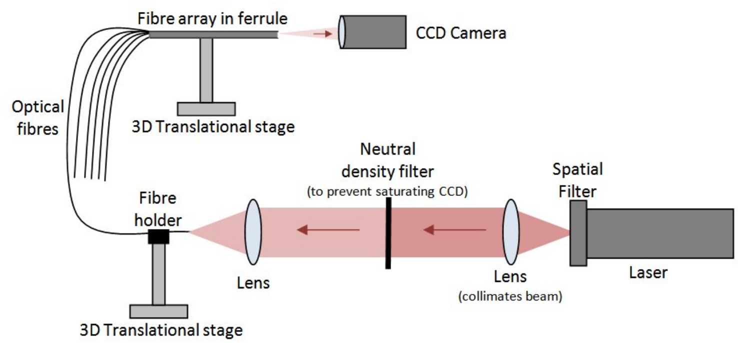

Figure 3.2: Camera setup for array characterisation tests. Laser is a 632nm red He Ne, spatial filter creates a uniform intensity diverging beam from this.

relative intensity throughputs of the fibres.

The array was fitted to a three-dimensional translation stage and pointed at a Unibrain Fire-i bbw 1.3 CCD camera, itself mounted on a tip-tilt stage. The camera lens was adjusted so that the camera was focused at a point a few centimetres in front of itself. The other ends of the fibres (the loose ends, not in an array) were prepared for maximum light coupling by stripping away 3cm of protective buffer then scribing and cleaving (as described in section 3.2.1) to give the fibre a flat uniform end. One of the fibres was then mounted in a fibre holder and had laser light from a 1.0mW He Ne laser focused into it (see figure 3.2), enabling the output of the fibre to be studied.

3.3.1 Relative Positions

The position of the fibre array was adjusted using the translation stage, until the end of the array was at the focus of the camera. The camera and array were then covered

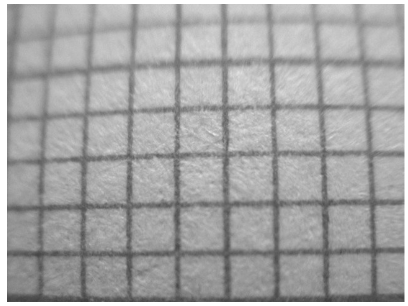

Figure 3.3: 1mm square graph paper imaged at focal point of camera in place of fibre array.

with black material to block out external light sources, and left in position.

The loose fibres were then illuminated one at a time and imaged using the CCD camera. A Python program was created to remove the averaged background frame (image of system with laser aperture closed) and convert the image to a FITS file so it could be analysed using DS9 image analysis software. The edge of the beam was defined as the point where the intensity dropped to $1/e^2$ of the maximum value. Contours of various smoothnesses were drawn around this boundary with the software and the centres of these contours were used to find the averaged centre point of the beam and the standard deviation of this value. In this way the inter-fibre spacing distance could be determined in terms of pixels as well as the deviation in alignment from a perfect linear array. To convert from pixels into mm, and to investigate distortions induced by the camera lens, a sheet of graph paper was placed at the focus of the camera.

The image of the graph paper, figure 3.3, shows a large amount of barrel distortion in the image, introduced by the lens. These effects can be largely ignored however as the image of the array falls only on the central squares, which are relatively distortion free. The pixel distance relations were found to be 78708±1604 pixels/m in the x direction and 77292±1669 pixels/m in the y direction.

3.3.2 Angle

The angle a fibre in the array was pointing at, relative to the other fibres in the array, was measured from the relative angles of the light exit cones. These were determined by moving back the array on the translation stage so the camera could image a plane of the light cone. The centre of the light cone was then found using the technique described above and these were compared with the coordinates of the fibre end points, from the relative positions data described in the previous section. The distance that the array had been retracted on the translation stage was read off the micrometer scale and used with the fibre end and exit cone coordinates to determine the exit angle and uncertainty on this measurement and thus the angle of the fibre in the array.

3.3.3 Intensity Throughput

To measure the relative throughputs of the fibres in the array, sufficient neutral density filters were inserted in the path of the laser beam, as it left the laser, so that the CCD would not be saturated for even the brightest (that with the best throughput) of the fibres in the array. The intensity measurements were all taken with the array in the 'retracted' position, so that the intensity was spread over a wide light cone and individual pixels were less likely to be saturated. Another Python program was created to sum the individual intensities of the pixels in the averaged background subtracted image, so the intensities could be quantified. The error in this intensity measurement was found by repeating the test on repeated images that had been taken at the time.

3.3.4 Coupling Error

The intensity measurement assumes that the maximum possible amount of light has been coupled in at the loose fibre input end. This maximum was judged by eye, by carefully adjusting the position and tip/tilt of the input end of the fibre until sufficient light was coupled to saturate the CCD. An additional neutral density filter was then put in the path of the laser beam so the CCD was no longer saturated and the fibre position finely adjusted to maximise the intensity further and attempt to saturate the CCD again. Neutral density features were continued to be added until the CCD could no longer be saturated at the maximum intensity position. The uncertainty on the assumption that this was the maximum was measured by repeating readings and adjusting the fibre and re-finding the supposed maximum coupling position each time.

3.4 Adjusting Path lengths

The optical fibre wavefront corrector will require a mechanism by which the individual fibres can be independently stretched. Previously work on fibre stretching within this project used a single computer controlled, rapidly altering piezo-electrical based fibre stretcher (see figure 3.4) to experiment on a single fibre [9].

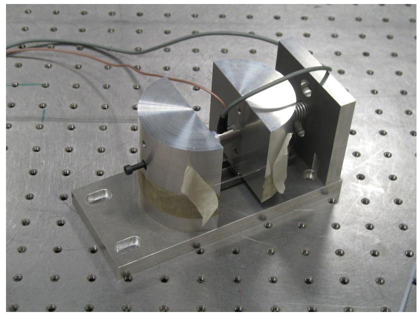

Figure 3.4: Computer controlled piezo-electric optical fibre stretcher.

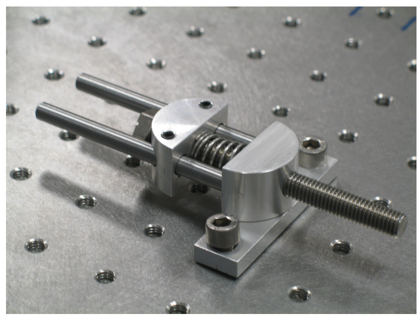

Figure 3.5: Fibre stretching device prototype.

For investigating arrays of fibres a stretcher is required for each fibre in the array and rapid stretching variations are not required until a full adaptive optics system is ready to be simulated. To this end a cheap and simple manually operated fibre stretcher is required.

A fibre stretching device was made from an aluminium cylinder cut along its length, with a large screw to adjust the separation between the two halves and a spring to maintain the tension, see figure 3.5. Unfortunately however the separation adjustment provided by this proved too crude to be useful for altering stretches (thus path lengths) by fractions of a wavelength. Instead then, a mirror mount with precise tip-tilt adjustment on its platform was used. With the platform at its lowest adjustment, the fibre was connected to the backing plate on one side and tightly

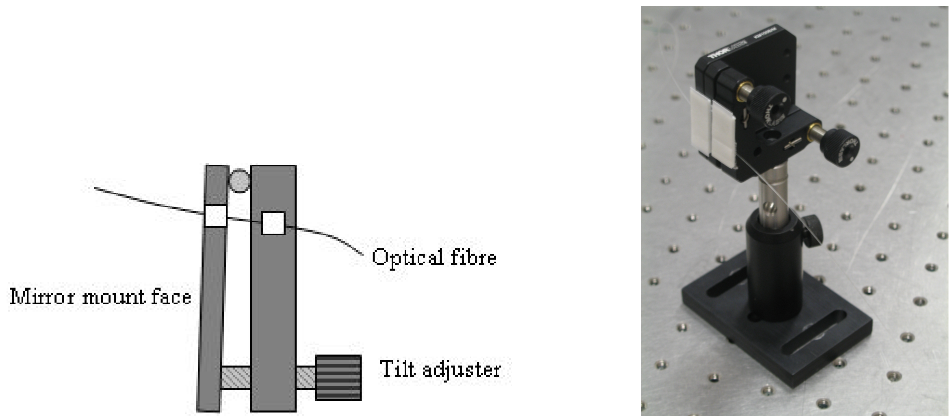

(a) (b)

Figure 3.6: Precision tip-tilt optical mount, adapted to become optical fibre stretcher.

to the tip-tilt platform on the other (where the mirror would usually be mounted) with adhesive foam pads (see figure 3.6). When this gap is increased, by adjusting the relevant tip or tilt screw, the fibre is stretched very slightly. The manual fibre stretcher was then tested using an interferometer setup.

3.5 Interferometer System

The interferometer setup is shown in figure 3.7. The collimated laser beam is split so that half the light is sent to the input to the fibre array, and the other half is recombined with the light exiting the fibre array. The laser beam is monochromatic and the coherence length is sufficiently long that even though the path lengths are different by a few metres, interference fringes are produced in the recombined light and imaged on the CCD camera. If interference fringes are not produced, then the phase information must somehow become scrambled in the array. The stability of the system is visible by the fringe drift (rate at which the interference fringes track

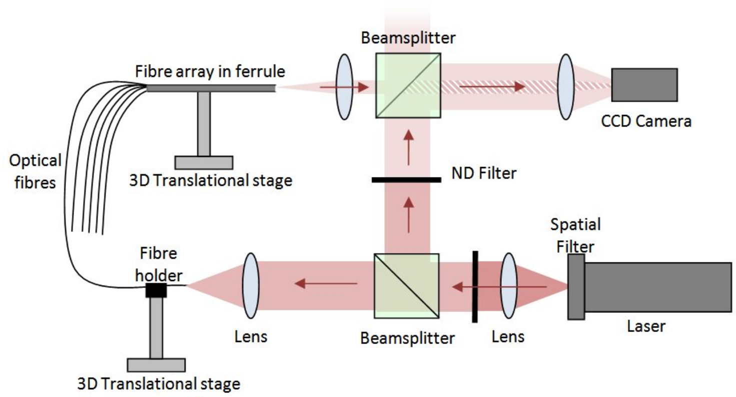

Figure 3.7: Interferometer setup.

across the screen, in a supposedly stable setup). Fringe drift was minimised in this investigation by using a floating optical table to reduce externally induced vibrations. Also the laser was left turned on throughout so it was always at operating temperature. Even so, small motions and body heat transferred when placing ones hands near the fibres was enough to subtly alter fibre positions and path lengths (on the scale of 632nm, the laser light wavelength) to create significant movement in the interference fringes.

3.6 Computer Simulation

Making accurately aligned arrays of single-mode fibres is a difficult and time consuming process. To predict the resulting outcome from any given array of fibres, from any given input, a computer program was made using Numerical Python to simulate arrays of single-mode fibres (see appendix). The program creates a construct, into which any number of fibre 'objects' can be loaded. The virtual fibres can emit light of any wavelength, intensity and phase, and can be placed at any

3D coordinate pointing in any direction (any tip and tilt angles) with any given exit angle (numerical aperture). The resulting interference patterns can be viewed on a screen of any given size and pixel resolution at any given distance along the z axis. The image formed on the virtual screen is then output as a FITS file.

To model this accurately requires complex electric field integrals to be solved. As an approximation however, the fibres were modelled as 'Fresnel' point sources, with an obliquity factor and numerical aperture applied to them, see section 2.5.1.

This method however is very computationally intensive, rendering ten high resolution images (at different z distance) of just ten fibres, can take several hours on a modern Pentium 4 based computer. The processing time could be reduced if more general approximations were used, e.g. using Fourier transforms, but these do not handle diffraction, and so would create a very poor approximation to the array output. The transport of intensity function is another approximation method that could be used, but that is only accurate near foci so again would not be appropriate.

To test the physics of the computer simulation, it was used to reproduce an approximation of the Young's slits interference experiment. The slits were represented by two parallel rows of closely spaced fibres at different z distances and had to be kept short to reduce the rendering time. Once the physics had been shown to be correct, the program was then used to create a model of a perfect linear array with 125μm spacings. The program was also used to create a model of the array that was actually produced, using the results obtained in the characterisation process described in section 3.3. The program was then adjusted to randomise the input variables for the virtual fibres within a Gaussian probability curve using the standard deviations of the values of the fibre positions and angles in a Monte Carlo style simulation. From this the uncertainty in the fringes created by the program due to the errors in the input data could be quantified. The fringe parameter measured for this was the angle the interference fringes, created from pairs of fibres in the array, made with the vertical.

Chapter 4

Results, Analysis and Discussion

The results of the experiments described in the previous chapter, looking first at the array produced and interferometry, then at the computer program to model it.

4.1 Array of single-mode Fibres

4.1.1 Design and Construction

The design specification of the array was ten linear and close packed fibres as described in section 3.1. The method of construction that was finally selected, was to assemble the fibres in line and glue, to place the array in a long ferrule, and to polish it with fibre polishing paper and is explained in section 3.2.2. The specifics of the construction method however took months to perfect and it still has much room for improvement. Producing an array of single-mode fibres is fiddly and has a low success rate. The final array used in this investigation does not represent the best possible array achievable with this technique, it is however the best the author could reasonably expect to make and analyse in the time available.

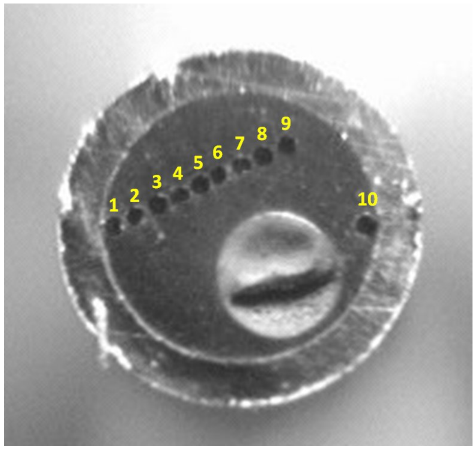

(a) Illuminated from front and numbered

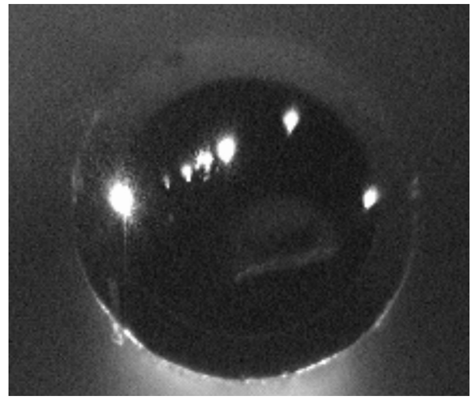

(b) Fibres illuminated.

Figure 4.1: End of fibre array, mounted in 2mm diameter stainless steel ferrule and polished. The large circle inside the ferrule is an air bubble in the optical glue.

The array created is shown in figure 4.1 with front illumination and with the fibres themselves illuminated from their other ends. It can be seen that not all the fibres transmit light, and that one has fallen out of line from the others. The general faults with each fibre in the array, as numbered in figure 4.1(a) are outlined in table 4.1.

Fibres, 2 and 7, show no intensity because the fibres have snapped completely and there are only the ends of them remaining in the array. The fibres snap because they become very brittle where the outer jacket layer is removed from them. The fibres with damaged ends, 5 and 8, do transmit light, but at a lower intensity and with a light distribution across the fibre end that is non-uniform (see figure 4.2(a)). Figures 4.2(b) and 4.2(c) show that the damage appears to be a breakage behind the front face of the fibre array, as the light seems to be diffused by the optical glue and

Table 4.1: Condition of fibres within the array

Fibre	**Issues**
1	None
2	snapped
3	None
4	No position data due to camera mis-alignment
5	Damaged end
6	None
7	snapped
8	Damaged fibre end
9	None
10	Fibre became separated from others when inserted into ferrule

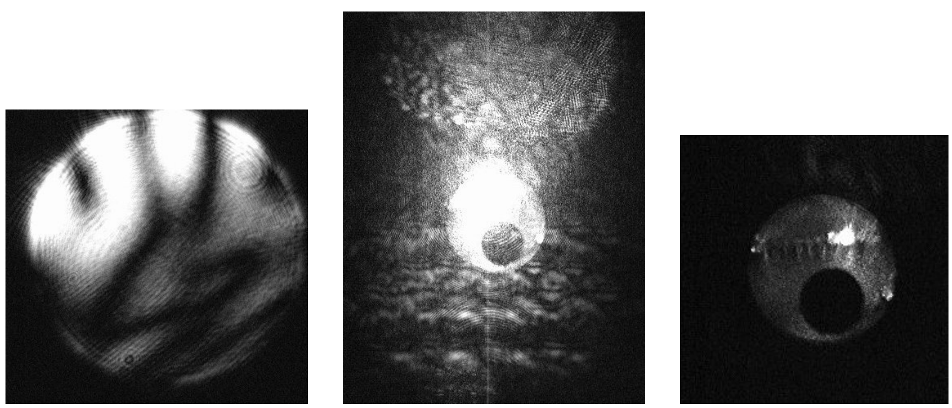

(a) Close up of end of fibre 8 showing non-uniformity of intensity.

(b) Fibre 5 with near maximum laser light coupled and no ND filter, hence CCD is saturated.

(c) Fibre 8 with near maximum laser light coupled, viewed through ND filter to show brightness distribution.

Figure 4.2: Damaged fibres within the array

the air bubble is creating a silhouette in the foreground.

4.1.2 Characterising Fibre Positions and Angles

To quantitatively assess the accuracy of the construction method and the quality of the array produced, the positions of the fibre ends in the array and the angles they were pointing at were characterised using the methods discussed in section 3.3. This data was later entered into the computer model to simulate the interference fringes that would be produced if all the fibres were working simultaneously.

The positions of the fibre cores and the errors on the positions are shown in figure 4.3. Figure 4.3(a) shows all the available fibres with equal scales on x and y axes, figure 4.3(b) shows just the linear section with the y axis scale expanded to show the deviations from linearity more clearly. Figure 4.4 shows the data in picture form, being a composite picture made from adding the photos used to obtain the data points in figure 4.3.

A linear fit was applied to the points in figure 4.3(b) and optimised by minimising chi squared. The average deviation from this fit in the y direction was found to be -2.6$\pm$1.1μm, the range of deviations being 9.7$\pm$3.6μm. This is reasonable considering a fibre core has a mode field diameter of 4.3μm, but there is clearly room for improvement and its suitability for the proposed wavefront corrector could not really be determined until an array-lenslet coupling test has been performed.

The spacings between the fibre cores were also determined from these measurements. Again, ignoring fibre 10, the average core spacing was found to be

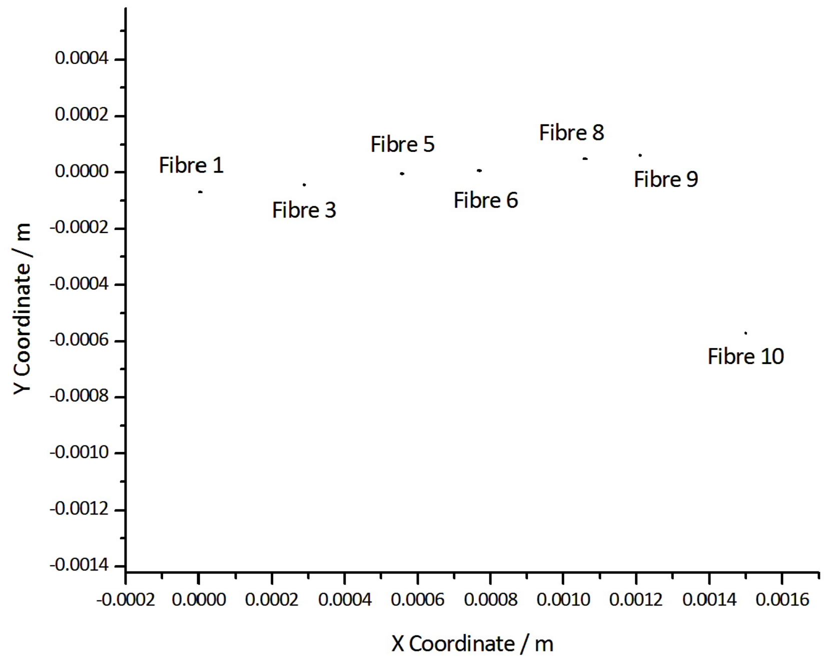

(a) Core positions of fibres 1,3,5,6,8,9,10

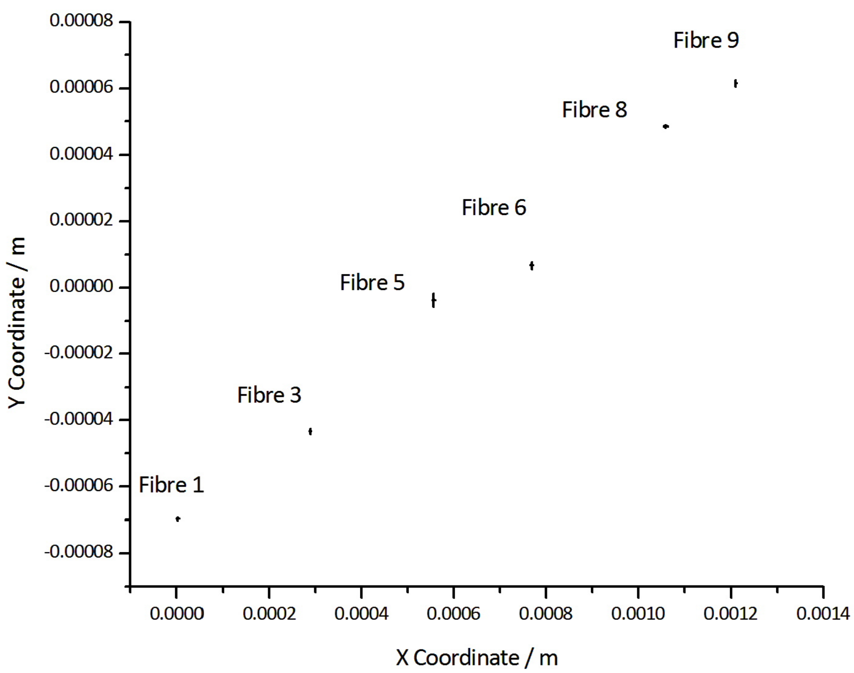

(b) Core positions of fibres in the linear section of the array only (i.e. not fibre 10)

Figure 4.3: Plots of the positions (with uncertainties) of the fibre cores at the end of the array.

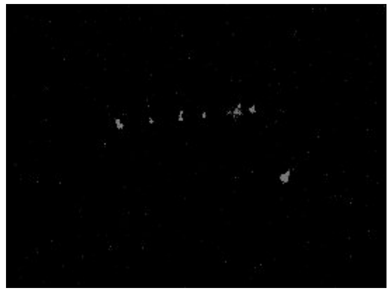

Figure 4.4: A composite image of all the separate, intensity normalised, fibre images. Contrast and brightness levels adjusted to reduce background noise.

150.6$\pm$3.7μm, the range of spacings being 17.7$\pm$7.2μm. This is larger than the design specification spacing of 125μm. It is clear from figure 4.1(a) that the main cause of the increased spacing is from gaps forming between the fibres, that appear to be filled with optical glue. These would arise because the fibres were not clamped in this direction when they were being assembled, though it is difficult to see how they could be. The extra spacing will present a problem for array-lenslet coupling, particularly for large arrays since the misalignment effect would be cumulative. A larger spaced lenslet array might be obtainable to compensate for this, alternatively silicon v-grooves as discussed in section 3.2.2 would provide a regular, lenslet compatible spacing if the other issues with them could be overcome.

The range of tip (up/down) angles was found to be 1.96$\pm$0.09 degrees, with the error on the average tip angle being 0.03 degrees. The range of tilt (side to side) angles was found to be 3.83$\pm$0.01 degrees, with the error on the average tilt angle being 0.03 degrees. This is well within the acceptance angle of the input coupling, which can be approximated from the quoted NA using equation 2.12 as 6.89$\pm$0.02 degrees, though the coupling will only be maximum when it falls on-axis [34]. The angle data is also required to replicate the array in the computer model, and is relevant to the output array fibre-lenslet coupling as when combined with core position it determines whether the output light falls over the centre of the lenslet or otherwise. For a lenslet lens with focal length 5.5mm, the range of y displacements of the light on a lens due to tip angle would be $188{\pm}9\mu$m, the range of x displacements due to tilt angle would be $368{\pm}1\mu$m. In the extreme cases the fibre could be pointing at a lenslet three along from the one it is supposed to be pointing at.

These angles could cause distortions in the image, because there would be a tilt across the aperture. Also light that falls between the lenslets would be lost from the system. In the full wavefront corrector it might be possible, to some extent, to calibrate out small distortions however.

4.1.3 Characterising relative throughput intensities

Figure 4.5 shows the range of intensities observed exiting the array when laser light from the same laser was coupled into the different fibres. The standard deviation on the average intensity is $\pm 82\%$. In an ideal array these intensities would all be equal, the fact that they are not is probably largely due to coupling conditions into and out of the fibres and indicates the varying quality of the polishing and cleaving, as well as the presence of broken ends as discussed in section 4.1.1. There is also a possibility that the neutral density filters performed differently if they were orientated differently or angled differently which would cast some doubt on these results. Also unless carefully aligned to be exactly on-axis with the camera lens the intensity across the light cone appeared to be non-uniform, see figure 4.6. The camera was re-aligned after each intensity throughput measurement to reduce this

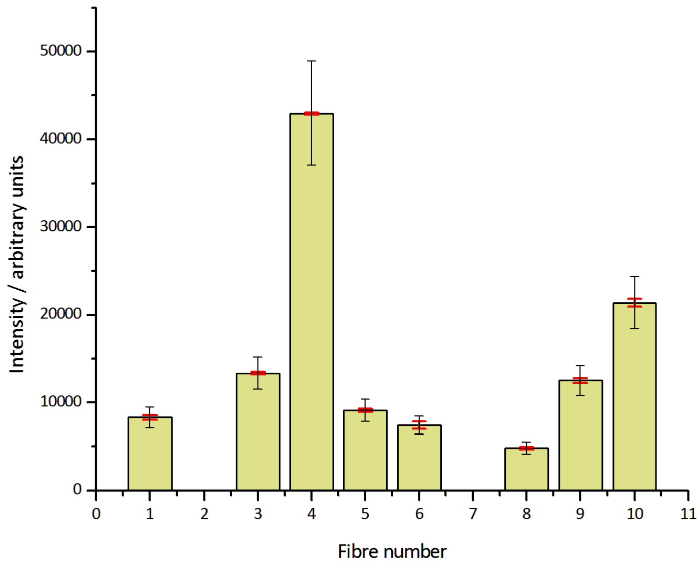

Figure 4.5: Relative Intensity throughputs between fibres. Red error bars indicate uncertainty on measurement, black error bars indicate range of values which could appear to be maximum when aligned by eye.

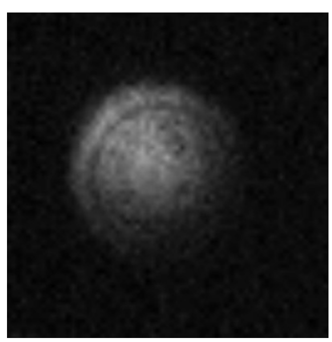

Figure 4.6: If light cone was viewed slightly off axis it would appear to have a non uniform brightness distribution, compared to a near uniform distribution when viewed on-axis.

as far as possible. Large intensity differences will create low contrast, and thus difficult to see fringes should the fibres be required to interfere (see section 2.5.2). In terms of the wavefront corrector varying throughputs for the fibres will cause errors in the brightness distribution of images produced. These varying throughputs can probably be overcome with improved fibre preparation methods.

As described in section 3.3.3 and section 3.3.4, there are two errors associated with the intensity values. The error on the measurement due to the detector/fluctuations in the laser intensity, and the uncertainty as to whether the maximum amount of light was being coupled into the fibre. The latter, the average coupling error is larger and perhaps more important and was found to be a $14 \pm 1\%$ uncertainty on 'maximum' intensity, i.e. the range of intensity values that could appear to be the maximum.

Since this coupling error is significantly larger than the error on the measurement, it would appear that the region in which the coupling is maximum, is smaller than the smallest adjustment of the fibre position. The adjustment screws moved the translation stage on which the fibre holder was mounted by $504.0 \pm 2.4\mu$m per turn, so each fractional turn of the adjuster moved the fibre by a few microns thus moving about the distance of the fibre core diameter.

Since the spacings between the fibres varied within a range of $17.7 \pm 7.2\mu$m and even if a lenslet array could be found to match the average spacing, it seems that very little, if any, of the light would be coupled into the fibre array. In terms of the wavefront corrector, these are construction issues which can probably be

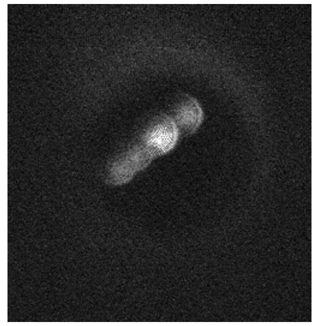

Figure 4.7: A digitally enhanced image of overlapping outputs from the array.

overcome. It does suggest however that the fundamental issue of tilts across lenslet subapertures (see section 2.3.1), will indeed be a big issue with the proposal and should be investigated more thoroughly.

4.1.4 Interferometry

If the laser is focused into two or more fibres simultaneously then where the beams exiting the array overlap, interference fringes should be observed. Without assembling the input fibre ends into an array it is difficult to achieve this. Figure 4.7 shows the image produced 4.5mm away from the array when the fibres were held in a bundle in the laser beam. There are no clear interference fringes. This is probably because the relative intensities between the fibres are quite different which reduces the contrast of the fringes, see section 2.5.2. Also because there is only a small amount of light passing through the fibres, the image is grainy so fainter fringes would not be visible.

If the fringes are not there at all, rather than just not visible in low light and low contrast conditions, then the spatial coherence of the laser light must somehow be

(a) Interfering beam off (b) Interfering beam on

Figure 4.8: Fibre 9, an undamaged fibre, examined with interfering beam.

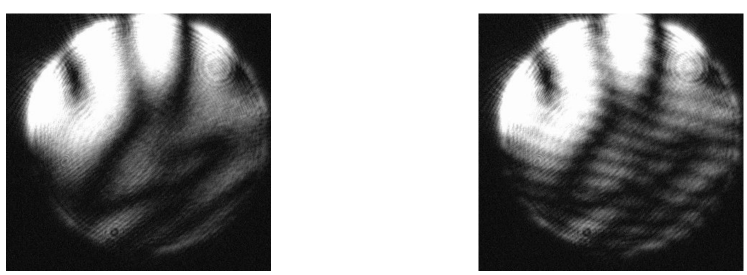

(a) Interfering beam off (b) Interfering beam on

Figure 4.9: Fibre 8, a damaged fibre, examined with interfering beam.

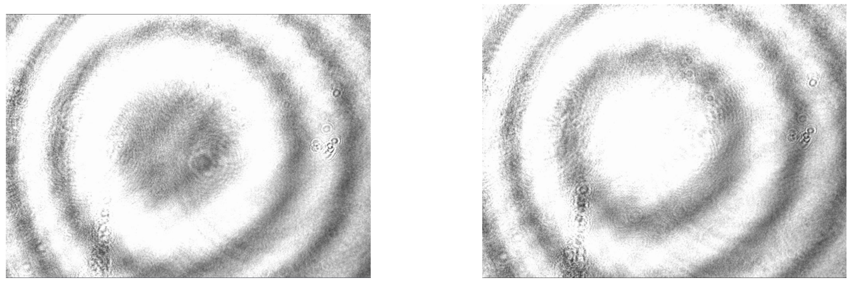

(a) (b)

Figure 4.10: Changing fringes observed when using fibre stretcher

lost in the fibre array. This is unlikely but could potentially be because the coherence length of the laser is too short, or perhaps light is travelling through the cladding and introducing modal pollution. To test for this, the interferometer described in section 3.5 was setup and used to interfere the light from the fibres individually with laser light that had not passed through the array. This setup produced clear fringes for even the fibres with damaged ends (see figures 4.8 and 4.9), proving that the spatial coherence is maintained and thus that the absence of visible fringes in figure 4.7 is likely to be due to low fringe contrast and image graininess.

Spatial coherence would be a requirement of the optical fibre wavefront corrector as precise knowledge and control are required of the relative path-lengths for each subaperture.

4.1.5 Stretching Fibres

The fibre stretcher designs described in section 3.4 were tested briefly in the interferometer setup. The adapted mirror mount design (figure 3.6) was found to have reasonably accurate control over fringe positions, but a small amount of fringe drift was still present. Frames from a video recording made of the interference fringes are shown in figure 4.10. The stretcher was not investigated further at this stage as it was not used in the rest of the investigation, but once an array is constructed and lenslets coupled, it could be used to test how stretches applied to individual fibres affect the output image. The fibre stretcher designs described in section 3.4 were tested briefly in the interferometer setup. The adapted mirror mount design (figure 3.6) was found to have reasonably accurate control over fringe positions, but a small amount of fringe drift was still present. Frames from a video recording made of the interference fringes are shown in figure 4.10. The stretcher was not investigated further at this stage as it was not used in the rest of the investigation, but once an array is constructed and lenslets coupled, it could be used to test how stretches applied to individual fibres affect the output image.

4.2 Computer Program

The computer program was written in Python and can model the image produced by any collection/array of single-mode fibres as a collection of Fresnel point sources with a numerical aperture applied to them, as described in section 3.6.

4.2.1 Young's Slits

The Young's slits experiment produced the images in figure 4.11. Figure 4.11(a) shows a direct image of the slits. As one moves away, the image becomes a Fourier transform of the slits as per Fraunhofer diffraction, see figures 4.11(b) and 4.11(c). As the two beams overlap clear interference fringes are visible, demonstrating that the computer model is working, see figures 4.11(d) and 4.11(e).

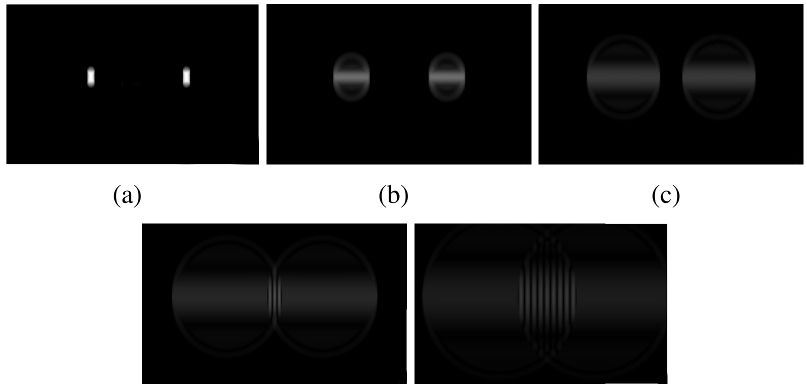

(a) (b) (c)

(d) (e)

Figure 4.11: Young's slits experiment as replicated within computer program. Successive images show the diffraction/interference patterns obtained as one moves away from the illuminated slits.

4.2.2 A Perfect Array

Figure 4.12 shows the results when a a perfect 125μm spaced array of seven fibres is input into the computer program. Figure 4.12(b) shows the point just after the adjacent fibres have started to interfere. The lenslet array would probably be inserted just before this. The subsequent images show how the interference fringes develop if the light from the fibres is not collimated and left to diverge.

4.2.3 The Real Array

The characterisation data of the fibre coordinates within the array, the fibre angles and relative intensities obtained in section 4.1.2 and section 4.1.3 were entered into the computer program, to produce a computer model of the real array that had been constructed. The images produced at increasing z distance are shown in figure 4.13. Figure 4.13(a) is essentially the position data from figures 4.3(a) and 4.4 combined with the intensities from figure 4.5. When this is combined with the angle data for

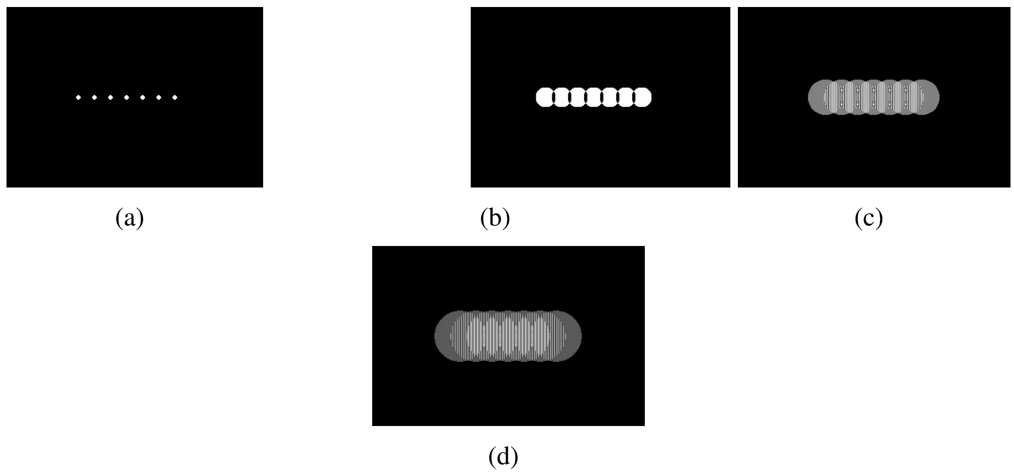

Figure 4.12: The computer model's representation of a perfect 125μm spaced array of seven fibres, viewed at increasing z distance.

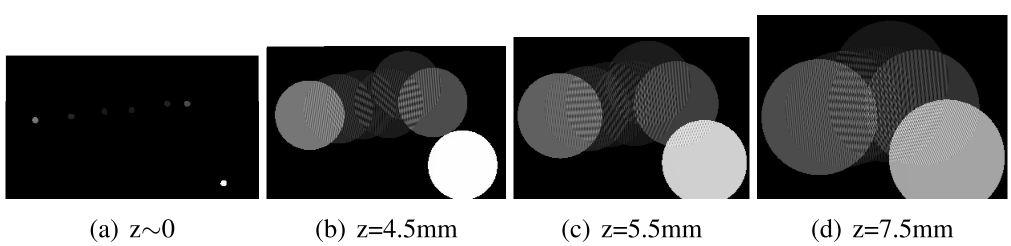

Figure 4.13: The computer model's representation of the fibre array created.

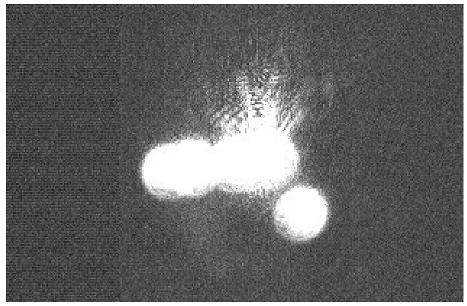

Figure 4.14: Composite image (hence no interference) of array at z=4.5mm

each fibre the subsequent figures can be produced. These subsequent figures show reasonably clear interference fringes even though the intensities are different.

The focal length of the lenslet array was found to be 5.54±0.08mm in section 3.1.2. Figure 4.13(c) shows the light cones at approximately this focal length so corresponds roughly to the light that would fall on the lenslet array. The size of the light cones are only approximations though as the numerical apertures are not exact (see section 2.4.1), but it seems clear that there will be a certain amount of overlap between lenslets. Weight is added to this argument by figure 4.14, which shows a composite image of the photos of the fibres at z=4.5mm. It shows that there is already an overlap at this distance and compares well with the computer model, figure 4.13(b), suggesting that the NA approximation is a reasonable one.

This is a bad sign for the project however. Even if the fibres are perfectly aligned, there is a mismatch between the focal ratio of the lenslet array and the fibre, so that if the lenslet array is placed at its focal length from the fibre array, light from adjacent fibres will spill into adjacent lenslets which is likely to have a detrimental effect on the output image. A lenslet array with a shorter focal length is required.

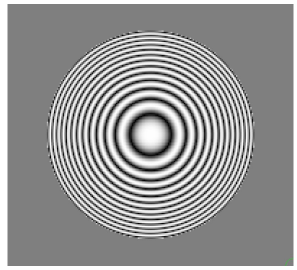

Figure 4.15: Computer program results of the overlapping light cones of two closely spaced fibres within the interferometer setup.

The uncertainty in the fringes created by the program due to the the errors on the input data was found using the Monte Carlo style simulation (see section 3.6). The standard deviation on the average fringe angles was measured for separate fibre pairs and averaged to give 1.0±0.1 degrees.

4.2.4 Interferometry

Additionally the interferometer was built into the computer program. Figure 4.15 shows the results for a single fibre within the interferometer setup. This is modelling the setup in 4.10 and figure 4.8(b). The reason figure 4.8(b) does not show circular fringes is because the optics were not perfectly aligned, as was the case for figure 4.10 and the computer simulation.

4.2.5 Limitations of Program

The computer program is only a model of the array and is not without its limitations. The wave propagation and interference is described by Fresnel geometric optics when in reality single-mode fibres are best described using electric and magnetic fields. Likewise the exit cones of the fibres in the virtual array are calculated by the Numerical Aperture (NA) quoted on the fibres data-sheet assuming the geometric optics relation in equation 2.12 holds. To be correct, the NA could have been calculated empirically from the photos of the fibre throughput in the retracted, wide light cone, position. The NA was not considered to be an important characteristic to include in the initial modelling program however, as it does not affect the fringes and the composite photo figure 4.14 and computer model figure 4.13(b) are in reasonable agreement. Also the program assumes that all the fibre ends have a uniform polish, unlike fibres 5 and 8 (see figures 4.2 and 4.9(b)). Random brightness variations across individual fibres would be difficult to model so the program uses the average intensity of the fibres instead.

Another somewhat limiting factor of the computer program is its processing time. As discussed in section 3.6, it takes a long time to perform the calculations required to display the effects of just a few fibres, and there are probably not many further time saving approximations that could be made without severely affecting its accuracy. For high resolution modelling of large arrays in a manageable amount of time then the program could be optimised in C and/or run on a supercomputer. If it were to be taken this far however one would want to be confident that it was going to give realistic results.

The true test of the computer model as it stands would be to create the conditions where the fringes in figure 4.13 could be observed on the real array to see if the two corresponded within the tight uncertainty quoted. This would require coupling sufficient coherent light into multiple fibres simultaneously to produce a non-grainy image, which was not possible with the experimental setup.

The computer program would appear to be working well, but further analysis of the real array is required to validate this. If it is found to be accurate the program could easily be expanded to model further parts of the proposed wavefront corrector.

Chapter 5

Conclusions

The findings of the investigation are summarised and evaluated below, extensions and follow up investigations are then discussed.

5.1 Summary of findings

A method was developed for creating passively aligned arrays of single-mode fibres, see section 3.2.2. A sample array was constructed and methods for characterising the placements, angles and intensity throughputs of the fibres within the array were developed, see section 3.3. Furthermore a computer model was created to model single-mode fibre output arrays and steps were taken toward wavefront correction with an array of single-mode fibre delay lines.

Linearity and Core Spacings

A close-packed linear array of ten single-mode fibres was created. One fibre became separated from the others during construction, two more snapped and the position results of another could not be used because of a camera mis-alignment. The remaining five were within a range of deviations from linearity of 9.7±3.6μm and had an average core to core spacing of 150.6±3.7μm, the range of spacings being 17.7±7.2μm, see section 4.1.2. This compares to a design specification spacing, and lenslet array lenslet pitch, of 125μm, see section 3.1. The increased spacing width would seem to arise because the fibres are not held or clamped along this axis during the curing process. In the y direction they were clamped with vernier callipers and hence the error in linearity is comparatively small.

Angles

Although it was not tested, it would seem that this fibre array would not couple well to the selected lenslet array since the core diameter that the lenslets have to focus into is ∼4.3μm and the fibre spacings are on average 25μm too wide. The effect is worsened by the fact that the fibres are all pointing in slightly different angles. The range of tip angles was found to be 1.96±0.09 degrees, with the error on the average tip angle being 0.03 degrees. The range of tilt angles was found to be 3.83±0.01 degrees, with the error on the average tilt angle being 0.03 degrees, see section 4.1.2. This is within the approximated acceptance angle 6.89±0.02 degrees, so at the input end of the array this in itself does not prevent coupling, though it will not be maximised. At an output array the tip and tilt angles of the fibre would further displace where the exit light cone falls on the lenslet array by an additional (to the core displacement) 368±1μm in the x direction and 188±9μm in the y direction. The size of the deviation angles may be reduce-able with improved clamping techniques during the array assembly and curing processes.

Intensities

The intensities were found to vary widely from fibre to fibre, the standard deviation on the average intensity being $\pm 82\%$, see section 4.1.3. This is attributable to the varying quality of the polishing and cleaving of the fibre ends, and the presence of broken and damaged fibres. The angle and orientation of the ND filter may have had an affect on these measurements as may have off-axis light loss effects associated with the camera lens, though efforts were made to minimise this.

Although the error on individual intensity measurements was small, there was a larger uncertainty as to whether the maximum amount of light was being coupled into the fibre. The error associated with this was found to be a $14 \pm 1\%$. This sensitivity in the positioning for maximum intensity confirmed that the optimum coupling position was at most a few microns across.

Interferometry

Interference fringes were not observed between adjacent output fibres because the experimental setup only allowed the laser light to be focused into single fibres. Only small amounts of light could be coupled into multiple fibres simultaneously. The spatial coherence of the light passing through the fibres in the array was confirmed however when interference fringes were observed using an interferometer setup to interfere laser light that had passed through the array, with light from the same source that had not passed through the array.

Computer Program

A computer program was written in Python which was able to model the interference patterns from any number of fibre output ends which can be placed at any 3D coordinate pointing in any direction. As well as being used to model an ideal array, the positions, angles and intensities data obtained of the real array was entered into the program to produce a model of the fringes that would have been produced if the laser light was coupled into multiple fibres. To assess how the uncertainties in the position and angles data affected the fringes in the program a Monte Carlo style simulation was run on the program, randomly changing the parameters according to their uncertainties. The uncertainty on the angle of the various fringes calculated was found to be 1.0 ± 0.1 degrees. The program was extended to be able to model the interferometer setup also.

5.1.1 Evaluation

Many questions remain as to whether the concept of wavefront correction with an array of single-mode fibre delay lines is workable, particularly the field of view issues explained in section 2.3.1 and in image reconstruction, but it was never in the scope of this investigation to answer all those. This investigation has demonstrated the difficulties involved with making the necessary fibre arrays and has determined where the manufacturing tolerances will cause problems and has provided the tools for further work on this project. Namely a method for creating arrays, techniques for characterising and analysing them, and software to model them.

5.2 Suggested further work

Create New Arrays

The first new array to create would be one at the input end of the current array. Laser light could be focused into it with a cylindrical lens and sufficient light might then be available for interference patterns to be observed at the array output, between adjacent light cones. Alternatively multiple setups of the single fibre coupling setup could be used, with multiple beam splitters used to split the laser light between them. The fringes predicted by the computer program could then be compared directly to those produced experimentally to thoroughly test the validity of the computer model and the approximations it makes. Difficulties may arise with balancing the intensities between fibres so the fringes are visible.

Beyond this improved linear arrays could be created, using improved clamping techniques, and 2D arrays may be possible, from stacking linear arrays or otherwise.

Lenslet Coupling

A lenslet array will not couple well to the array created in this investigation, but lenslet coupling will need to be investigated on future arrays. A more straightforward experiment would be to couple a single fibre to a lenslet and investigate how coupled light intensity varies with the angle off axis of an incoming collimated beam. Fibres with tapered ends could also be investigated as they have higher coupling efficiencies [35], or photonic crystal fibres, which have larger core diameters also [36]. Once suitable fibre arrays have been produced this experiment could be extended to examine the field of view effects in 1D and 2D arrays and image reconstruction. Alongside this the computer program could be expanded to also model the lenslet array, perhaps as an array of phase additions to the light from the array.

Fibre Delay Lines

Once input and output arrays are setup the fibres between them can be tested as delay lines using the manual fibre stretcher developed in this investigation. The relative phases between fibres could be viewed with the interferometer setup, and net tips and tilts to the entire wavefront could be added by the manual stretchers to tip and tilt the whole image produced at the output. Once this is arranged, automated fibre stretchers could be brought in and a demonstration AO setup constructed.

Chapter 6

Acknowledgements

Many thanks to Dr Richard Myers and Dr Tim Morris for their constant help and support, bright ideas and wisdom they provided throughout this investigation.

Also thanks to Juergan Schmoll for his assistance with the lenslet metrology, Graham Murray for his help and advice with optical fibres and silicon v-grooves, and Alastair Basden for help with the report printing.

References

[1] Beckers JM, *Adaptive Optics for Astronomy: Principles, Performance, and Applications*, Annu. Rev. Astron. Astrophys. **31**:13-62 (1993).

[2] Lambert, *J. PixelOptics to Develop SuperVision for U.S. Military*, http://www.asd-network.com/press_detail_B.asp?ID=6486, viewed 05/01/2007

[3] adaptiveoptics.org, *AOptix Technologies Introduces AO-Based FSO Communications Product*, http://www.adaptiveoptics.org/News_060_1.html, viewed 05/01/2007

[4] adaptiveoptics.org, *Retinal OCT Imaging System to Incorporate Adaptive Optics*, http://www.adaptiveoptics.org/News_0406_2.html, viewed 05/01/2007

[5] Love GD, *Adaptive Optics*, Astronomical Optics Lecture Course, Durham University (2006)

[6] Morris TJ, *High-Order Wavefront Correction using Variable Optical Fibre Delay Lines*, Unpublished material, Durham University, (2003)

[7] M. Puech, F. Hammer, P. Jagourel, E. Gendron, F. Assemat, F. Chemla, H. Flores, P. Laporte, J.-M. Conan, T. Fusco, A. Liotard, F. Zamkotsian, *FALCON: Extending adaptive corrections to cosmological fields*, New Astronomy Reviews **50** 382384 (2006)

[8] Greenaway AH, *Optical aperture synthesis*, Meas. Sci. Technol. **2** 1-12 (1991)

[9] Morris S, *Wavefront Correction Using Fibre Optic Delay Lines (fibre response)*, MSci thesis, Durham University, (2006)

[10] Perrin G, Lacour S, Woillez J, Thibaut , *High Dynamic Range Imaging by Pupil Single-mode Filtering and Remapping*, Mon. Not. R. Astron. Soc. **373**, 741-751 (2006)

[11] J.W. Hardy, *Adaptive Optics For Astronomical Telescopes*, Oxford University Press, 1998

[12] Fried DL, *Statistics of a Geometric Representation of Wavefront Distortion*, J. Opt. Sci. Am, Vol. **55**, Issue 11, pp. 1427- (1965)

[13] Tokovinin A, *Adaptive Optics Tutorial*, CERRO TOLOLO INTER AMERICAN OBSERVATORY, http://www.ctio.noao.edu/ atokovin/tutorial/intro.html, viewed 09/01/07

[14] McGregor P, *Adaptive Optics Systems Layout*, Research Network for Adaptive Optics, http://www.mso.anu.edu.au/rnao/images/AOlayout.jpg viewed 13/01/07

[15] Law NF & Lang RG, *Wavefront Estimation at Low Light Levels*, Optics Communications, **126** (1-3): 19-24 May 1 (1996)

[16] Thompson LA, Castle RM *Experimental demonstration of a rayleigh-scattered laser guide star at 351-nm*, Optics Letters **17** (21): 1485-1487 Nov 1 (1992)

[17] Lloydhart M, Angel JRP, Jacobsen B *et al. Adaptive Optics Experiments using sodium laser guide stars*, Astrophysical Journal **439** (1): 455-473 Part 1 (1995)

[18] Myers RM, Longmore AJ, Benn CR, Buscher DF, *et al.* , *NAOMI adaptive optics system for the 4.2m William Herschel telescope, Adaptive Optical System Technologies II*, Proc. SPIE, Volume **4839**, pp. 647-658,(2003)

[19] Hecht E, *Optics - Fourth Edition*, Addison Wesley, 2002.

[20] Tipler PA, Mosca G, *Physics for Scientists and Engineers - fifth edition, extended edition*, WH Freeman and Company, 2004.

[21] Thor Labs, *SM600 Specification Sheet*, http://www.thorlabs.com/thorcat/12600/12605-M01.pdf, viewed 21/04/2007

[22] Shaklan S and Roddier F, *Coupling starlight into single-mode fiber optics*, Appl. Opt. **27**, pp.2334-2338, (1988)

[23] Perrin G, Lena P, Foresto VC, Lai O, *A fibered large interferometer on top of Mauna Kea - OHANA, the optical Hawaiian array for nano-radian astronomy*, Interferometry in optical astronomy; Proceedings of the Conference, Munich, Germany; 27-29 Mar. 2000. pp. 708-714. (2000)

[24] Simohamed LM, Delage L, Reynaud F, *An optical fibre delay line with a 318 mm stroke*, Pure Appl. Opt. **5** 1005-1009, (1996)

[25] Answers.com, *Multimode Fiber*, http://www.answers.com/topic/multimode-fiber, viewed 23/04/2007

[26] [Ghatak and Thyagarajan (1989)] Ghatak AK & Thyagarajan K, *Optical Electronics*, Cambridge niversity Press, 1989

[27] Ishikawa K, Zhang J, Tuantranont A, Bright VM, Lee CY, *An integrated micro-optical system for VCSEL-to-fiber active alignment*, Sens Actuators A Phys **103**:109-115 (2003)

[28] Rose GJ, Davis DW, *Precision fiber optic array connector and method of manufacture*. Microsystem Technologies, Volume **12**, Numbers 10-11, 965-972, September, (2006)

[29] Chanclou P, Gravey P, Bonnel L, Thaul M, *Matrix 8 x 8 single-mode fibers with micro-optics*, Optics Communications **198** 121-123 (2001)

[30] Law SH, Phan TN, Poladian L, *Fibre geometry and pigtailing*, Electronic Components and Technology Conference, 2001. Proceedings., 51st Pages:1447 - 1450, (2001)

[31] Weiland D, Luetzelschwab M, Desmulliez MPY, *Two-dimensional monomode optical fibre array manufacture using microengineering techniques* Microsyst Technol **12**: 965-972 (2006)

[32] Longhurst RS, *Geometrical and Physical Optics, Second Edition*, Longmans, 1967

[33] Chang MPJL and Buscher DF, *Cleaving optical fibre lengths to high relative accuracy*, Opt. Comms. **157**, 282-290 (1998)

[34] Cheo PK, *Fiber Optics & Optoelectronics, second edition*, Prentice-Hall International Inc, 1990.

[35] Jarmolik A, Vandeputte K, VanHove A, VanDaele P, *Effective coupling from semiconductor lasers to single mode fibers*, Optica Applicata **26** (4): 369-374 (1996)

[36] Corbett J, Dabirian A, Butterley T, Mortensen NA, Allington-Smith JR, *The coupling performance of photonic crystal fibres in fibre stellar interferometry*, Mon. Not. R. Astron. Soc. **368**, 203-210 (2006)

Appendix A

Single-mode fibre array Python program